

University of Denver

Digital Commons @ DU

Center for Orthopaedic Biomechanics: Faculty
Scholarship

Center for Orthopaedic Biomechanics

1-2024

Simultaneous Evaluation of Tibiofemoral and Patellofemoral Mechanics in Total Knee Arthroplasty: A Combined Experimental and Computational Approach

Yashar A. Behnam

Ahilan Anantha Krishnan

Hayden Wilson

Chadd W. Clary

Follow this and additional works at: https://digitalcommons.du.edu/orthopaedic_biomechanics_faculty



Part of the [Biomechanical Engineering Commons](#), [Biomechanics Commons](#), and the [Biomechanics and Biotransport Commons](#)



This work is licensed under a [Creative Commons Attribution 4.0 International License](#).

Simultaneous Evaluation of Tibiofemoral and Patellofemoral Mechanics in Total Knee Arthroplasty: A Combined Experimental and Computational Approach

Publication Statement

Copyright is held by ASME. User is responsible for all copyright compliance. This article was originally published as:

Behnam, Y. A., Anantha Krishnan, A., Wilson, H., and Clary, C. W. (2024). Simultaneous evaluation of tibiofemoral and patellofemoral mechanics in total knee arthroplasty: A combined experimental and computational approach. *Journal of Biomechanical Engineering*, 146(1), 011007. <https://doi.org/10.1115/1.4063950>

Accepted Manuscript is openly available through the "Download" button.

The published Version of Record is available at libraries through Compass or Worldcat.

Publication Statement

Copyright is held by ASME. User is responsible for all copyright compliance. This article was originally published as:

Behnam, Y. A., Anantha Krishnan, A., Wilson, H., and Clary, C. W. (2024). Simultaneous evaluation of tibiofemoral and patellofemoral mechanics in total knee arthroplasty: A combined experimental and computational approach. *Journal of Biomechanical Engineering*, 146(1), 011007. <https://doi.org/10.1115/1.4063950>

Accepted Manuscript is openly available through the "Download" button.

The published Version of Record is available at libraries through Compass or Worldcat.

Simultaneous Evaluation of Tibiofemoral and Patellofemoral Mechanics in Total Knee Arthroplasty: A Combined Experimental and Computational Approach

Yashar A. Behnam

Department of Mechanical and Materials Engineering
The University of Denver,
2155 E. Wesley Ave.
Denver, CO 80210
Yashar.Behnam@du.edu

Ahilan Anantha Krishnan

Department of Mechanical and Materials Engineering
The University of Denver,
2155 E. Wesley Ave.
Denver, CO 80210
Ahilan.Ananthakrishnan@du.edu

Hayden Wilson

Department of Mechanical and Materials Engineering
The University of Denver,
2155 E. Wesley Ave.
Denver, CO 80210
Hayden.Wilson@du.edu

Chadd W. Clary¹

Department of Mechanical and Materials Engineering
The University of Denver,
2155 E. Wesley Ave.
Denver, CO 80210
Chadd.Clary@du.edu

ABSTRACT

Contemporary total knee arthroplasty (TKA) has not fully restored natural patellofemoral (P-F) mechanics across the patient population. Previous experimental simulations have been limited in their ability to create dynamic, unconstrained, muscle-driven P-F articulation while simultaneously controlling tibiofemoral (T-F) contact mechanics. The purpose of this study was to develop a novel experimental simulation and validate a corresponding finite element model to evaluate T-F and P-F mechanics. A commercially available wear simulator was retrofitted with custom fixturing to evaluate whole-knee TKA mechanics with varying patella heights during

¹ Please direct all questions, comments, and inquiries to Chadd Clary at Chadd.Clary@du.edu

a simulated deep knee bend. A corresponding dynamic finite element model was developed to validate kinematic and kinetic predictions against experimental measurements. Patella *alta* reduced P-F reaction forces in early and mid-flexion, corresponding with an increase in T-F forces that indicated an increase in extensor mechanism efficiency. Due to reduced wrapping of the extensor mechanism in deeper flexion for the *alta* condition, peak P-F forces in flexion increased from 101% to 135% of the applied quadriceps load for the *baja* and *alta* conditions, respectively. Strong agreement was observed between the experiment and model predictions with root mean square errors (RMSE) for P-F kinematics ranging from 0.8° to 3.3° and 0.7 mm to 1.4 mm. RMSE for P-F forces ranged from 7.4 N to 53.6 N. By simultaneously controlling dynamic, physiological loading of the T-F and P-F joint, this novel experimental simulation and validated model will be a valuable tool for investigation of future TKA designs and surgical techniques.

INTRODUCTION

Total knee arthroplasty (TKA) is the most common treatment for end-stage osteoarthritis and other degenerative diseases of the knee. Restoring patients' natural joint kinematics is important for patient satisfaction, joint stability, and implant survivorship [1,2]. While most studies on TKA mechanics focus on the tibiofemoral (T-F) joint, patellofemoral (P-F) mechanics directly influence patient satisfaction and knee stability following TKA [1–4], while patellar mal-tracking and pain are common causes of revision [2,5,6]. *In vivo* P-F mechanics are influenced by quadriceps muscle forces and lines of action, resection of the patella and implant alignment, the articulating geometry, repair of the lateral retinaculum, and T-F kinematics [4,5,7,8]. Development and testing of new TKA components to improve patient function typically requires experimental simulation using joint loading experienced *in vivo* to enable pre-clinical measurement of dynamic knee kinematics and stability. Realistic knee mechanics requires simultaneous loading of the T-F and P-F articulations in a physiologically relevant manner.

Early whole knee experimental simulators, like the Oxford-style knee loading rig, used a linear actuator attached to the quadriceps tendon to counteract a vertical load applied through the hip [9]. This style of simulator allows unconstrained movement at the knee, including the P-F joint, but is limited in its ability to control loading in each of the knee's degrees of freedom (DoF) simultaneously and independently. Advancements to Oxford-style rigs include the addition of loaded degrees of freedom at the ankle to simulate approximated ground reaction forces and control systems to simulate dynamic activities [10,11]. In contrast, robotic-arm based systems leverage the end-effector of a robotic arm coupled with a loadcell to apply kinematics to the knee while measuring the resulting joint loads. Recently, robotic simulators have included cables with weights or actuators to simulate muscle forces [12–17]. Robotic-systems have the unique ability to independently control loading in each of the knee's degrees of freedom but are limited in their

capacity to apply dynamic force-controlled loading to the knee as seen in common activities of daily living [12,18,19].

Some physical limitations of experimental simulators can be overcome using computational models. Advancements in finite element (FE) analysis and musculoskeletal modeling have led to improved computational tools to predict knee mechanics and are commonly used during the pre-clinical evaluation of new TKA designs [20–22]. These models can evaluate component designs under dynamic loading conditions that would otherwise be difficult and costly to achieve experimentally. Godest et al. developed a finite element model replicating the Stanmore knee simulator and verified the resulting kinematics against the experiment [23]. Guess et al. developed a multibody dynamic model of the Kansas Knee Simulator. Their model was verified against predictions for patellar tendon load, and ranges of motion for T-F adduction-abduction (Ad-Ab) rotation, internal-external (I-E) rotation, and medial-lateral (M-L) translation [24]. Baldwin et al. similarly developed a finite element model of the Kansas Knee Simulator verified through comparisons with the 6 DoF P-F and T-F kinematics, and actuator loading during deep knee bend and gait activities. Such models incorporate sophisticated control systems that approximate the human neuromuscular system [25–27] and tissue representations that enable the prediction of ligament tensioning and bony remodeling [28,29].

As these models' capabilities exceed their experimental counterparts, model validation becomes challenging and limits applications in regulatory filings. The purpose of the current study was to develop a novel experimental simulator to evaluate knee mechanics, capable of simultaneous dynamic load-control of both T-F and P-F joints, and to experimentally validate a corresponding FE model to complement the experimental measurements.

METHODS

VIVO Joint Simulator Modifications

A commercially available, servo-hydraulic, six degree-of-freedom VIVO joint simulator (AMTI, Watertown, MD) was retrofitted with custom fixturing and a secondary actuator to enable whole knee joint loading (Fig. 1, *left*). The VIVO joint simulator was originally designed for tribological testing of TKA, thus includes a control system that can apply simultaneous physiologically relevant loading conditions at the knee via the tibia and femur in either load or displacement control. The functionality of the VIVO was augmented by replacing the standard femoral Ad-Ab arm of the simulator with a custom assembly that enables attachment of cadaveric or synthetic femurs, with adjustability in the Ad-Ab, I-E, M-L, and anterior-posterior (A-P) femoral anatomic axes to facilitate alignment of the specimen relative to the mechanical axes of the simulator.

The custom fixturing enabled simulation of the quadriceps musculature via a linear ball screw actuator (Thomson, Radford, VA) driven by a servo motor in a belt-coupled parallel configuration and was controlled via a servo drive (Kollmorgen, Norwalk, CT). The quadriceps actuator line of action (*Q-angle*) could be adjusted $\pm 15^\circ$ from the femoral superior-inferior (S-I) axis. A uniaxial load cell (Cooper Instruments & Systems, Warrenton, VA) fixed to a custom quadriceps tendon clamp measured quadriceps force in line with the muscle actuation (Fig. 2, *left*). Programming and data acquisition of the corresponding control system were implemented in LabVIEW (National Instruments, Austin, TX). The control system leveraged a proportional-integral-derivative (PID) control scheme to apply either constant or dynamic quadriceps loading profiles synced to the VIVO's integrated control system. The PID controller was tuned via the Ziegler-Nicol's method [30] and manually adjusted to optimize the load-tracking response.

Synthetic Knee Assembly

While the fixturing can accommodate cadaveric tissue, the system performance was initially evaluated on a synthetic knee to enable benchmarking performance and to simplify subsequent finite element model development. A synthetic 3D-printed femur and tibia were

implanted with a commercially available fixed-bearing cruciate-retaining TKA components and mounted into the simulator, with the femur attached to the upper stage and the tibia attached to the lower stage (Fig. 1, *middle*). The synthetic bones were designed in CAD software (Solidworks, Dassault Systemes, Vélizy-Villacoublay, France) such that the origin of the femur implant's coordinate system (the intersection of vectors pointing superiorly from the most distal point and anteriorly from the most posterior point on the femur's articulating surface) was coincident with the intersection of the simulator's flexion-extension (F-E), Ad-Ab, and I-E axes with the simulator in the neutral alignment. Likewise, the femur implant's axes were rotationally aligned parallel to the simulator's axes in full extension. The synthetic tibial bone housed a slot coinciding with the tibial tuberosity to attach a Kevlar® strap that simulated the quadriceps tendon. The synthetic bones were 3D printed from ABS plastic (Fortus 450mc, Stratasys, Rehovot, Israel).

The Kevlar straps were affixed to the tibial tuberosity of the tibial bone and to the distal end of a patella fixture to represent a patellar ligament (Fig. 1, *right*). Straps of three different lengths were used to represent natural variation in patella tendon length (Fig. 2, *right*): *baja* (40-mm patella tendon), *neutral* (60-mm patella tendon), and *alta* (80-mm patella tendon), corresponding to Blackburne-Peel ratios of 0.5, 0.8, and 1.0, respectively [8]. The proximal end of the patellar fixture was attached to the quadriceps clamp via a second length of the same Kevlar strap. The patella fixture was implanted with a medialized dome patella and included a piezoelectric triaxial loadcell (Kistler, Novi, MI, Fig. 2, *middle*) mounted below the patella articulation to measure M-L, A-P, and S-I P-F forces.

Implant kinematics were tracked with an active-marker optical tracking system (OPTOTRAK Certus HD, Northern Digital, Waterloo, Canada) at a rate of 100Hz. Rigid arrays were affixed to each implant fixture to measure both T-F and P-F kinematics [31]. Tibial bone loading was measured at the base of the tibial fixturing via a six DoF loadcell incorporated in the

AMTI VIVO, and joint moments and forces from the loadcell were transformed to a virtual coordinate system at the knee's center. These loading measurements were synced with loadcell data from the quadriceps actuator and patella implant fixture. After assembly and alignment, an optical scan of the experimental configuration was performed (SpaceSpider, Artec 3D, Luxembourg) to enable precise measurement of the implant positions and quadriceps actuator orientation relative to the optical tracking arrays and simulator axes.

Knee Experimental Simulations

A series of controlled loading conditions were applied to the synthetic bones to investigate force transfer through the knee and to enable subsequent computational model validation with a *neutral* patellar tendon length. During the isolated quadriceps loading profile, a quadriceps load was applied via the quadriceps tendon following a cosine waveform ranging from 100 N to 1000 N at 15°, 30°, 45°, and 60° knee flexion. During quadriceps loading, a tibial compressive load of 200 N was held constant, and the remaining DoF at the knee (I-E, Ad-Ab, M-L, A-P) maintained zero force or torque in load control. The 200 N compressive load was sufficient to maintain bi-condylar contact of the knee implants while still allowing translation of the tibia relative to the femur in response to the quadriceps loading. Three cycles of the sinusoidal loading profile were applied and the P-F reaction force at peak loading was averaged across cycles.

During the simple deep knee bend (DKB), a 500 N quadriceps load was applied through the quadriceps tendon as the knee dynamically flexed and extended following a cosine wave from 0° to 80° while a 200 N compressive load was applied to the tibia. Although smaller than the quadriceps loads typically observed during a DKB in vivo, the 500 N quadriceps load was sufficient to ensure articulation between the femur and patella while not overloading the triaxial loadcell embedded below the patella. The tibial I-E rotation was constrained at 0° in displacement control and the remaining tibiofemoral axes (A-P, M-L, and Ad-Ab) were maintained at zero

force or torque. Five cycles were performed for each loading condition at a rate of 0.015 Hz while T-F and P-F loads and kinematics were recorded. T-F kinematics were further analyzed by calculating the location of the closest points on the femur implant's medial and lateral condyles to the plane of the tibial resection (i.e., lowest-points). Kinematics and loadings were averaged across cycles. The simple DKB loading conditions were repeated with the patella in *alta* and *baja* positions.

Computational Model Formulation and Validation

A dynamic FE model of the experimental setup was developed in Abaqus Explicit (Dassault Systèmes, Vélizy-Villacoublay, FR, Fig. 1, *right*) based on a previously verified model of a stock AMTI VIVO simulator [32]. The simulator's fixtures, synthetic bones, and implants were meshed using triangular shell elements (Type: S3R) and modeled as rigid bodies. The mean edge length for non-articulating components (bones and fixtures) was 1.5 mm while the edge length for the articulating implant elements was 0.5 mm based on a previously published convergence study on knee kinematics [33]. The total number of surface elements in the model were 145,480 (non-articulating components) and 147,727 (articulating components). Contact interactions between the femur, patella, and tibial implants were defined using a previously verified pressure-overclosure relationship with a friction coefficient of 0.04 [20].

The straps representing the quadriceps ligament and patella tendon were modeled as deformable quadrilateral membrane elements (Type: M3D4R) with an axial length of 6 mm and transverse width of 3 mm (140 total elements). The membrane elements were reinforced with link-type connector elements (Type: CONN3D2, link) along the strap axis, thus making the strapping inextensible. The proximal and distal ends of the patella ligament strap were attached to the patella fixture and tibial tuberosity, respectively, via hinge connector elements (Type: CONN3D2, hinge) to allow relative rotation in the sagittal plane. Likewise, the distal end of the quadriceps tendon was attached to the proximal aspect of the patella fixture in the same fashion and the proximal end was

attached to the quadriceps actuator. The experiment's quadriceps actuator was modeled with a corresponding connector element (Type: CONN3D2, translator). A final connector element was embedded between the patella implant and the patella fixture (Type: CONN3D2, bushing) to measure the loads experienced by the patella during contact with the femur corresponding with the 3-axis loadcell used in the experiment.

The loads applied to the knee by the VIVO simulator in the experiment were controlled via virtual coordinate systems aligned to the implant geometry using a three-cylindric open chain configuration described by Grood and Suntay [31]. To recreate the applied loading, a series of three mutually orthogonal connector elements (Type: CONN3D2, cylindrical) were aligned to the same virtual coordinate systems in the model. The first connector element was affixed to the tibia along the tibial S-I axis and oriented to allow S-I translation and I-E rotation of the knee. The second connector element was affixed to the M-L axis of the femur and oriented to allow M-L translation and F-E rotation of the knee. The third connector element connected the first two virtual axes and was oriented along a vector mutually orthogonal to both axes, coinciding with A-P translation and Ad-Ab rotation of the knee. Load-sensing connector elements (Type: CONN3D2, bushing) were embedded between the distal end of tibial S-I axis and the tibial bone to measure the loading experienced by the tibia corresponding to the 6-axis tibial load cell in the experimental set-up and between the tibial tray and insert to measure the T-F reaction forces. Note that the tibial reaction force and T-F contact force are different due to the forces exerted on the tibia by the patella tendon. A virtual proportional-integral (PI) control system was incorporated into the FE model that replicated the control algorithm of the experimental simulator. Forces and moments measured by the tibial load-sensing bushing were inputs to the PI controller via a user subroutine (VUAMP) and used to control load profiles for the connectors modeling the VIVO's actuators. The control system's proportional and integral gain parameters were tuned via a previously published method [34].

The meshed model was virtually aligned in the initial position relative to the VIVO simulator using the optical scan of the experimental setup thereby ensuring proper alignment of the fixtured assembly with respect to the simulator's actuators. Anatomic coordinate systems were defined in the model on the femur, tibia, and patella components using equivalent definitions to the experiment, which facilitated a direct comparison of T-F and P-F kinematics throughout the analyses. The same experimental boundary conditions were evaluated in the model, including the isolated quadriceps loading with the *neutral* patella position and the simple DKBs with the patella in *baja*, *neutral*, and *alta* positions. During each simulation, patella loads and knee kinematics were compared against the experimental measurements, and the Root Mean Square errors (RMSE), normalized Root Mean Square Error (nRMSE), mean errors (ME), and standard deviations (STD) of the differences were calculated.

Computational Model Sensitivity Analysis

Unlike the single synthetic bone used in the experimental component of this study, there is significant variability in quadriceps mechanism geometry across the potential patient population that affects knee mechanics. A model sensitivity analysis was performed to quantify the effect of variability in the quadriceps mechanism on uncertainty in the resulting kinematics and joint loads. The five alignment parameters considered in the sensitivity were the A-P position of the patellar tendon insertion, the patella *alta-baja* position (controlled by the patella tendon length), the patella composite thickness, the quadriceps muscle sagittal plane angle (controlled by the A-P position of the superior attachment of the quadriceps actuator), and the quadriceps muscle frontal plane angle (Q-angle, controlled by the M-L position of the superior attachment of the quadriceps actuator, Fig. 3). Based on published studies of extensor mechanism geometry across the patient population, the standard deviation from the mean for these alignment parameters were 2.5 mm, 5.0 mm, 3.0 mm, 2.5°, and 2.5°, respectively [7,35–37].

Perturbations in the alignment parameters were applied to the model's nominal alignment with the *neutral* patella position using the Monte Carlo method with sampling from normal distributions via Latin Hypercube Sampling (100-trials). The resulting T-F and P-F kinematics and loads during the simple DKB were evaluated. The range of flexion during the simulated DKB was extended to 120° flexion to quantify deep flexion behavior not measured experimentally. Correlation coefficients and corresponding slopes between the five input quadriceps variables and output knee mechanics were calculated. Output variables included P-F kinematics, P-F loading, T-F S-I loading, patella tendon load, quadriceps moment arm, and quadriceps elongation at 15°, 60°, and 120° knee flexion. The quadriceps moment arm was calculated by dividing the quadriceps elongation over a 6° flexion window centered on the flexion angle of interest by the corresponding change in flexion (in radians).

RESULTS

Isolated Quadriceps Loading

Peak experimentally measured P-F loading coincided with the maximum 1000 N applied quadriceps muscle force (Fig. 4). The primary component of the P-F loading was along the patella's anterior axis, increasing from 127.2 N at 15° flexion (12.7% of the quadriceps load) to 963.5 N at 60° flexion (96.4% of the quadriceps load, Fig. 4). Smaller components of the P-F reaction force (<111 N) were observed in the lateral and inferior directions through flexion. Equivalent loading patterns were observed in the FE model, with average RMSEs of 9.1 N, 46.8 N, and 27.2 N across all knee flexion angles in the M-L, A-P, and S-I axis, respectively. RMSE, nRMSE, ME, and STD of differences between the experiment and model for each degree of freedom are reported in Table 1.

Simple Deep Knee Bend

During the simplified DKB, the tibia translated posteriorly and rotated externally relative to the femur with increasing flexion for all patella conditions (Fig. 5). Increasing the patella tendon length (i.e., patella *baja* to patella *alta*) caused increased posterior translation of the tibia relative to the femur during peak flexion, with peak posterior translations of 4.1 mm and -3.0 mm for *baja* and *alta* conditions, respectively (Fig. 5). Tibial posterior translation with flexion was accompanied by external tibial rotation that was greater for the patella *alta* condition (2.2°) than the *baja* condition (3.4°). The tibial external rotation with flexion was the result of an anterior translation of the medial condyle on the tibial plateau as the knee flexed, which increased from -5.4 mm to 1.7 mm with a longer patella tendon (Fig. 6). The lateral condyle also experienced increased anterior translation on the lateral plateau in the patella *alta* condition.

The FE model T-F kinematic predictions were similarly sensitive to changes in patella tendon length, predicting the same increased posterior translation of the tibia in the patella *alta* condition as observed experimentally (Figs. 5-6). Overall RMSEs for kinematic predictions across patella conditions were less than 3.3° and 1.4 mm (Table 2). T-F V-V rotations and S-I translations achieved the best prediction accuracies, with average RMSE of 0.4° and 0.3 mm, respectively. The worst prediction accuracies were for T-F I-E and M-L, with average RMSE of 1.6° and 1.6 mm, respectively. RMSE, nRMSE, ME, and the STD of the model and experimental differences for each degree of freedom can be found in Table 2. Femoral low point translation predictions were most accurate when predicting S-I translations and least accurate for predicting M-L translations, for both the medial and lateral condyle. Average RMSEs for A-P translation were 1.0 mm and 0.9 mm across all patella configurations and each condyle, respectively (Table 3).

P-F kinematics demonstrated greater patella flexion relative to the femur in the patella *baja* condition (Fig. 7). Likewise, an evident discontinuity in the P-F A-P kinematics was observed when the *alta* patella entered the proximal trochlear groove, which did not occur in

either *neutral* or *baja* conditions as the patella was already articulating within the trochlear groove at full extension. In all conditions, the patella translated medially relative to the femur with increasing flexion, and P-F I-E rotation was negligible. These trends were also observed in the FE model, resulting in accurate kinematic predictions through the flexion range (Fig. 8). RMSEs in FE model P-F kinematics predictions across all conditions were less than 3.3° and 1.4 mm (Table 2). The best prediction accuracies were achieved for P-F V-V rotations and A-P translations, with average RMSE of 1.2° and 0.8 mm, respectively. The worst prediction accuracies were for P-F I-E and M-L, with average RMSE of 2.8° and 1.3 mm.

P-F loading during the simplified DKB followed similar patterns to the isolated quadriceps loading profiles, with the P-F A-P reaction force increasing with knee flexion (Fig. 9). Increasing the patella tendon length (patella *alta*) resulted in larger peak A-P forces, ranging from 470 N to 653 N for *baja* and *alta* cases, respectively. Increasing the patella tendon length also caused the S-I component of the P-F reaction force to change from -109 N in the inferior direction to 176 N in the superior direction for *baja* and *alta* conditions, respectively. In the *neutral* patella configuration, the S-I load oscillated between superior during flexion and inferior during extension, likely due to friction at the P-F articulation. P-F M-L reaction forces were consistently the smallest in magnitude and acted in the lateral direction. RMSEs in FE model P-F force predictions averaged 21 N and ranged between 7.4 N and 53.6 N across patella heights (Table 4). RMSE, nRMSE, ME, and the STD of the differences in model and experimental P-F loads for each degree of freedom can be found in Table 4.

Model Sensitivity Analysis

The model's sensitivity to the variation in the quadriceps geometry changed through flexion (Fig. 10). Variation in the tuberosity A-P position had no significant correlations (correlation coefficients > 0.6) with knee mechanics. Patella *alta* was directly correlated to P-F superior translation through flexion and to P-F M-L translation in mid-flexion due to articulating

higher in the angled trochlear groove. Likewise, patella *alta* caused an increase in the superior component of the P-F reaction force that propagated through the patella tendon, causing higher T-F S-I loading (7.6 N/mm of increased patella *alta*). In deep flexion, patella *alta* caused reduced P-F flexion and more anterior loading through the patella. Increased patella thickness was directly correlated with more anterior P-F translation. This caused an increase in the quadriceps moment arm in early and mid-flexion along with increased quadriceps elongation to reach mid and deep flexion (additional 1.5 mm of elongation per 1.0 mm of increased patella thickness). Increased patella thickness was also strongly correlated to higher P-F superior loading which propagated through the patella tendon into T-F compressive load. The sagittal angle of the quadriceps had weak correlations with P-F kinematics in extension that dissipated with increasing flexion. Likewise, increased sagittal quadriceps angle reduced P-F loading in early and mid-flexion. The frontal plane angle of the quad was strongly correlated with P-F M-L translation and V-V rotation in extension, prior to full engagement with the trochlear groove, and an increase in the P-F M-L reaction force once the patella was constrained within the trochlear groove in mid and deep-flexion.

DISCUSSION

The purpose of this study was to develop a novel whole knee loading apparatus capable of controlling six DoF T-F loads while simultaneously loading the P-F joint through a simulated quadriceps mechanism. To expand the capabilities of the experiment, a complementary FE model was developed that incorporated the same mechanisms and control system as the physical rig and was validated against the experimental measurements. The model accurately predicted changes in T-F and P-F mechanics when altering the patella height during a simplified DKB activity. The integrated control system of the complementary FE model will be used to develop increasingly sophisticated boundary conditions that enable future cadaveric simulation of patient-specific and implant-specific whole knee loading conditions.

Effects of patella height

While the primary focus of the study was model development and validation, the variations in patella height tested in the experiment provided insight into patellar mechanics and extensor mechanism efficiency. Patella *baja*, or pseudo-patella *baja*, is a common complication of TKA and has been associated with poor outcomes [38–42]. Multiple studies have demonstrated the effects of patella height on patella kinematics, patella loading, and extensor mechanism efficiency with conflicting results [43–46]. In a similar experimental study, Luyckx et al. developed an oxford-style knee loading apparatus and evaluated TKA P-F contact forces with different patella heights [44]. Unlike the current study, the quadriceps load was variable to create a constant vertical ground reaction force at the ankle and not held at a constant value (e.g., 1000 N). Between 30° to 70° knee flexion, patella *alta* resulted in lower P-F contact forces compared to patella *baja*, indicating an increase in the extensor mechanism efficiency. Ward et al. compared extensor efficiency in vivo between healthy subjects with normal or *alta* patellae using magnetic resonance imaging and observed that patella *alta* caused an increase in the effective moment arm of the extensor mechanism from 0° to 60° knee flexion [46]. In contrast, Tischer et al. [45] investigated TKA P-F mechanics using a musculoskeletal model and found patella *alta* resulted in an increase in patella contact force that persisted through the full flexion range.

In the current study, the patella *alta* condition had lower P-F reaction forces between 20° and 50° knee flexion coupled with higher T-F joint compressive loads (Fig. 11), indicating more quadriceps force was being transmitted from the quadriceps actuator through the patella, and into the patella tendon. Beyond approximately 60° flexion, wrapping of the quadriceps strap on the femur's trochlear groove was observed in the *neutral* and *baja* conditions, which offloaded the patella articulation. As a result, the patella *alta* condition had the highest PF reaction forces at 80° flexion of 135% of the applied quadriceps load, compared to 110% and 101% for the *neutral* and *baja* conditions. Similarly, the model sensitivity analysis identified direct correlation between

patella *alta* and the superior component of the P-F reaction force in mid-flexion, which propagated into an increased T-F reaction force. Although not directly calculated, an increase couple between the patella tendon force and T-F reaction force would increase the knee extension moment resulting in increased extensor efficiency. These results are consistent with the findings of Luyckx et al. [44] and Ward et al. [46] that patella *alta* improves extensor mechanism efficiency through mid-flexion but also increases patella loading in deeper flexion.

Prediction accuracy

T-F and P-F FE model prediction errors in the current study were less than 3.3° and 2.1 mm for knee rotations and translations, respectively. Errors for T-F A-P translations ranged from 0.5 mm – 2.1 mm across patella heights, while T-F I-E errors ranged from 1.7° - 2.2° . These accuracies are comparable to previous literature-reported studies with FE models of experimental knee simulators. In our previous work, we formulated a simpler FE model of the VIVO simulator configured for knee tribological testing [47]. When modeling the rigidly fixtured femur and insert, RMS errors were less than 1.7 mm and 1.4° for T-F A-P translation and I-E rotation, respectively. The accuracy in the current study was similar despite the increased modeling complexity of the quadriceps mechanism and compliance in the larger mechanical components of the simulator. Baldwin et al. predicted implanted P-F kinematics in cadaveric specimens loaded with the Kansas Knee Simulator and achieved an accuracy of 1.6 mm and 2.6° for P-F translations and rotations, respectively [32]. In a subsequent study using the same experimental set-up, Baldwin et al. simultaneously predicted implanted T-F and P-F kinematics in cadavers performing a DKB, achieving RMS errors of 2.1 mm and 1.3° for T-F A-P translation and I-E rotation, respectively [48]. Unlike the current study, kinematic predictions in cadaveric tissue require modeling the knee's ligaments and patella retinaculum. While this adds complexity to the model, it also enables tuning the soft tissue properties to recreate the measured knee kinematics

more closely. Future work using cadaveric tissue to develop patient specific computational soft-tissue models will further enhance the capabilities of the combined tool developed here.

Developing more meaningful boundary conditions

List et al. reported fluoroscopically measured *in vivo* T-F kinematics during a stand-to-sit activity for the same implant system analyzed in the current study [49]. During *in vivo* flexion, the medial condyle exhibited 3.2 mm of anterior translation coupled with a 1.2 mm posterior translation of the lateral condyle, causing approximately 5° external rotation of the femoral component relative to the tibia. The kinematics of the simplified DKB in the current study exhibited 5 mm of anterior translation of the medial condyle for the *neutral* patella height. However, the lateral condyle also translated 1 mm anterior with flexion and the medial condyle began approximately 4 mm more posterior in extension, resulting in a net 7°-8° relative internal rotation of the femur through the flexion range. Differences between the *in vivo* and *in vitro* kinematics are likely due to the simplified loading conditions used in this study.

A DKB simulation was performed with no transverse plane loading applied via the tibial actuator (e.g., no I-E torques or A-P forces) to enable model validation. The applied T-F compressive load and quadriceps load were lower than those typically experienced during an *in vivo* DKB [4]. There is a lack of comprehensive knee loading conditions in the literature, including quadriceps loading profiles, to drive these types of simulations. Previous studies have used telemetric implant data [50,51] or standardized profiles for wear testing (e.g., ISO 14243-2). The resultant T-F loading reported in these studies was a combination of ground reaction forces applied through the tibia and muscle loading. Further, the loading data derived from the highly conforming articular geometry of the telemetric implant may not be appropriate for evaluating moderately conforming contemporary implants. These limitations highlight the need for additional musculoskeletal modeling and profile optimization to generate realistic knee kinematics in future work. The combined experimental and computational platform validated in

the current study, combined with fluoroscopically measured knee kinematics, will be ideally suited to address this limitation.

Limitations and Future Work

In addition to the simplified boundary conditions, the current study was limited by using a fixtured TKA and synthetic extensor mechanism with different mechanical properties to human tendons. Although the fixtures were designed to directly mimic the bony and implant alignment of cadaveric knees within the simulator, the lack of realistic soft tissue limits the relevance of these findings to clinical scenarios. This simplification was deemed necessary to enable detailed FE model verification, including measurement of P-F contact forces. Future studies using cadaveric tissue and more sophisticated boundary conditions will likely require additional calibration of the ligament and tendon mechanical properties to accurately predict kinematics of native and implanted knees. Extending these experimental and computational methods into cadaveric tissue will illustrate the effects of morphological variations between subjects (e.g., patella tendon attachment site, patella thickness, patella *alta-baja*), ligament contributions to knee kinematics, and the influence of surgical technique.

An additional limitation of the current study was that knee flexion was limited to 80° due to the fixturing design and limitations in the simulator's range of motion. While this range of motion is sufficient to simulate most activities of daily living (e.g., gait, stair descent) and international standards for mechanical wear testing of TKA components (e.g. ASTM F3141 [52] and ISO 14243-1:2009 [53]), high flexion activities of daily living (e.g. chair-rise, chair-sit, and lunge) would require repositioning of the implants to test in one test cycle. Therefore, future studies will investigate fixturing modifications to achieve greater knee flexion to evaluate high flexion activities such as chair-rise, chair-sit, and lunging.

While TKA is widely considered a safe and effective treatment for knee arthritis, shortcomings in patient satisfaction have been well documented [54,55] and merit additional research. There is debate in the literature about the role of implant alignment (i.e. mechanical alignment versus kinematic alignment) in restoring soft tissue tensioning to healthy levels and the effect on patient satisfaction [56]. Further, complications of the P-F joint continue to be a significant cause of revision [54,55]. The combined experimental and computational whole joint simulator developed in this study provides a means to interrogate the roles of implant design and alignment in the detailed mechanics of the T-F and P-F joints during activities of daily living.

Through the future development of T-F and quadriceps loading profiles that recreate *in vivo* knee kinematics, surgeons and engineers will be able to investigate numerous challenges in contemporary joint arthroplasty. These studies are enabled by the ability of the simulator to simultaneously control T-F loading and P-F loading and the enhanced prediction capabilities of the complementary FE model. Specifically, these tools can be used to evaluate how changes in articular constraints (i.e. variable insert conformity or post-cam mechanisms) affect knee stability during dynamic activities of daily living. The tools can be used to investigate how patellar resection alignment and patella design affect quadriceps mechanics and T-F kinematics. The tools can be used to evaluate the relationship between implant alignment philosophy, ligament tensioning, and their combined effects on patellar tracking. Further, the validated complementary FE model provides the ability to evaluate these questions *in silico* prior to running expensive experiments.

Conclusions

The combined experimental and computational models developed in this study accurately predicted T-F and P-F mechanics and represent a significant step forward in our ability to simulate knee mechanics. This testing platform will be a valuable tool for engineers and surgeons to evaluate future novel TKA designs and surgical techniques. The variations in patella height

studied in this experiment demonstrated that patella *baja* reduces extensor mechanism efficiency in early and mid-flexion but reduces patella femoral loading in deeper flexion through increased wrapping of the quadriceps tendon along the anterior aspect of the femur. Future work will focus on the development of improved loading conditions to simulate activities of daily living in cadaveric tissue.

FUNDING

Funding for this study was provided in part by DePuy Synthes Joint Reconstruction, a Johnson & Johnson Company

REFERENCES

- [1] Australian Orthopaedic Association National Joint Replacement Registry (AOANJRR)., 2018, “Hip, Knee & Shoulder Arthroplasty: 2018 Annual Report. Adelaide: AOA, 2018.”
- [2] Sharkey, P. F., Hozack, W. J., Rothman, R. H., Shastri, S., and Jacoby, S. M., 2002, “Insall Award Paper. Why Are Total Knee Arthroplasties Failing Today?,” *Clin. Orthop. Relat. Res.*, (404), pp. 7–13.
- [3] P.M., B., A., K., M., C., C., C., C.U., G., S.F., H., B., W., D.E., O., and J.E., D., 2017, “Unusually High Rate of Early Failure of Tibial Component in ATTUNE Total Knee Arthroplasty System at Implant-Cement Interface,” *J. Knee Surg.*, **30**(5), pp. 435–439.
- [4] Sharma, A., Leszko, F., Komistek, R. D., Scuderi, G. R., Cates, H. E., and Liu, F., 2008, “In Vivo Patellofemoral Forces in High Flexion Total Knee Arthroplasty,” *J. Biomech.*, **41**(3), pp. 642–648.
- [5] Browne, C., Hermida, J. C., Bergula, A., Colwell, C. W., and D’Lima, D. D., 2005, “Patellofemoral Forces after Total Knee Arthroplasty: Effect of Extensor Moment Arm,” *Knee*, **12**(2), pp. 81–88.
- [6] Piedade, S. R., Pinaroli, A., Servien, E., and Neyret, P., 2009, “Revision after Early Aseptic Failures in Primary Total Knee Arthroplasty,” *Knee Surgery, Sport. Traumatol. Arthrosc.*, **17**(3), pp. 248–253.
- [7] Mizuno, Y., Kumagai, M., Mattessich, S. M., Elias, J. J., Ramrattan, N., Cosgarea, A. J., and Chao, E. Y. S., 2001, “Q-Angle Influences Tibiofemoral and Patellofemoral Kinematics,” *J. Orthop. Res.*, **19**(5), pp. 834–840.
- [8] Salem, K. H., and Sheth, M. R., 2021, “Variables Affecting Patellar Height in Patients Undergoing Primary Total Knee Replacement,” *Int. Orthop.*, **45**(6), pp. 1477–1482.
- [9] Zavatsky, A. B., 1997, “A Kinematic-Freedom Analysis of a Flexed-Knee-Stance Testing Rig,” *J. Biomech.*, **30**(3), pp. 277–280.
- [10] Navacchia, A., Clary, C. W., Han, X., Shelburne, K. B., Wright, A. P., and Rullkoetter, P. J., 2018, “Loading and Kinematic Profiles for Patellofemoral Durability Testing,” *J. Mech. Behav. Biomed. Mater.*, **86**(June), pp. 305–313.
- [11] Maletsky, L. P., and Hillberry, B. M., 2005, “Simulating Dynamic Activities Using a Five-Axis Knee Simulator,” *J. Biomech. Eng.*, **127**(1), pp. 123–133.
- [12] Noble, L. D., Colbrunn, R. W., Lee, D. G., Van Den Bogert, A. J., and Davis, B. L., 2010, “Design and Validation of a General Purpose Robotic Testing System for Musculoskeletal Applications,” *J. Biomech. Eng.*, **132**(2).
- [13] Grantham, W. J., Aman, Z. S., Brady, A. W., Rosenberg, S. I., Lee Turnbull, T., Storaci, H. W., Dornan, G. J., and LaPrade, R. F., 2020, “Medial Patellotibial Ligament Reconstruction Improves Patella Tracking When Combined With Medial Patellofemoral Reconstruction: An In Vitro Kinematic Study,” *Arthrosc. - J. Arthrosc. Relat. Surg.*, **36**(9), pp. 2501–2509.
- [14] D’Lima, D. D., Townsend, C. P., Arms, S. W., Morris, B. A., and Colwell, C. W., 2005, “An Implantable Telemetry Device to Measure Intra-Articular Tibial Forces,” *J. Biomech.*, **38**(2), pp. 299–304.
- [15] Navacchia, A., Bates, N. A., Schilaty, N. D., Krych, A. J., and Hewett, T. E., 2020, “Force During Landing Through the Posterior Slope of the Tibia,” **37**(8), pp. 1730–1742.
- [16] Willing, R., Moslemian, A., Yamomo, G., Wood, T., Howard, J., and Lanting, B., 2019, “Condylar-Stabilized TKR May Not Fully Compensate for PCL-Deficiency: An In Vitro Cadaver Study,” *J. Orthop. Res.*, **37**(10), pp. 2172–2181.
- [17] Herrmann, S., Woernle, C., Kaehler, M., Rachholz, R., Souffrant, R., Zierath, J., Kluess, D., and Bader, R., 2012, “HiL Simulation for Testing Joint Stability after Total Knee Arthroplasty,” *Multibody Syst. Dyn.*, **28**(1–2), pp. 55–67.
- [18] Lee, T. Q., 2014, “Biomechanics of Hyperflexion and Kneeling before and after Total

- Knee Arthroplasty,” *Clin. Orthop. Surg.*, **6**(2), pp. 117–126.
- [19] Bates, N. A., Nesbitt, R. J., Shearn, J. T., Myer, G. D., and Hewett, T. E., 2015, “A Novel Methodology for the Simulation of Athletic Tasks on Cadaveric Knee Joints with Respect to In Vivo Kinematics,” *Ann. Biomed. Eng.*, **43**(10), pp. 2456–2466.
- [20] Halloran, J. P., Easley, S. K., Petrella, A. J., and Rullkoetter, P. J., 2005, “Comparison of Deformable and Elastic Foundation Finite Element Simulations for Predicting Knee Replacement Mechanics,” *J. Biomech. Eng.*, **127**(5), pp. 813–818.
- [21] Hume, D. R., Navacchia, A., Rullkoetter, P. J., and Shelburne, K. B., 2019, “A Lower Extremity Model for Muscle-Driven Simulation of Activity Using Explicit Finite Element Modeling,” *J. Biomech.*, **84**, pp. 153–160.
- [22] Navacchia, A., Hume, D. R., Rullkoetter, P. J., and Shelburne, K. B., 2019, “A Computationally Efficient Strategy to Estimate Muscle Forces in a Finite Element Musculoskeletal Model of the Lower Limb,” *J. Biomech.*, **84**, pp. 94–102.
- [23] Godest, A. C., Beaugonin, M., Haug, E., Taylor, M., and Gregson, P. J., 2002, “Simulation of a Knee Joint Replacement during a Gait Cycle Using Explicit Finite Element Analysis,” *J. Biomech.*, **35**(2), pp. 267–275.
- [24] Guess, T. M., and Maletsky, L. P., 2005, “Computational Modelling of a Total Knee Prosthetic Loaded in a Dynamic Knee Simulator,” *Med. Eng. Phys.*, **27**(5), pp. 357–367.
- [25] Navacchia, A., Rullkoetter, P. J., Schütz, P., List, R. B., Fitzpatrick, C. K., and Shelburne, K. B., 2016, “Subject-Specific Modeling of Muscle Force and Knee Contact in Total Knee Arthroplasty,” *J. Orthop. Res.*, **34**(9), pp. 1576–1587.
- [26] Wagner, H., Boström, K. J., de Lussanet, M. H. E., de Graaf, M. L., Puta, C., and Mochizuki, L., 2022, “Optimization Reduces Knee-Joint Forces During Walking and Squatting: Validating the Inverse Dynamics Approach for Full Body Movements on Instrumented Knee Prostheses,” *Motor Control*, pp. 1–18.
- [27] Razu, S. S., and Guess, T. M., 2018, “Electromyography-Driven Forward Dynamics Simulation to Estimate in Vivo Joint Contact Forces during Normal, Smooth, and Bouncy Gaits,” *J. Biomech. Eng.*, **140**(7), pp. 1–8.
- [28] Harris, M. D., Cyr, A. J., Ali, A. A., Fitzpatrick, C. K., Rullkoetter, P. J., Maletsky, L. P., and Shelburne, K. B., 2016, “A Combined Experimental and Computational Approach to Subject-Specific Analysis of Knee Joint Laxity,” *J. Biomech. Eng.*, **138**(8), pp. 1–8.
- [29] Anijs, T., Eemers, S., Minoda, Y., Wolfson, D., Verdonschot, N., and Janssen, D., 2022, “Computational Tibial Bone Remodeling over a Population after Total Knee Arthroplasty: A Comparative Study,” *J. Biomed. Mater. Res. - Part B Appl. Biomater.*, **110**(4), pp. 776–786.
- [30] Ziegler, J. G., and Nichols, N. B., 1993, “Optimum Settings for Automatic Controllers,” *J. Dyn. Syst. Meas. Control. Trans. ASME*, **115**(2B), pp. 220–222.
- [31] Grood, E. S., and Suntay, W. J., 1983, “A Joint Coordinate System for the Clinical Description of Three-Dimensional Motions: Application to the Knee,” *J. Biomech. Eng.*, **105**(2), pp. 136–144.
- [32] Fitzpatrick, C. K., Maag, C., Clary, C. W., Metcalfe, A., Langhorn, J., and Rullkoetter, P. J., 2016, “Validation of a New Computational 6-DOF Knee Simulator during Dynamic Activities,” *J. Biomech.*, **49**(14), pp. 3177–3184.
- [33] Halloran, J. P., Petrella, A. J., and Rullkoetter, P. J., 2005, “Explicit Finite Element Modeling of Total Knee Replacement Mechanics,” *J. Biomech.*, **38**(2), pp. 323–331.
- [34] Fitzpatrick, C., Baldwin, M., Clary, C., Maletsky, L., and Rullkoetter, P., 2014, “Evaluating Knee Replacement Mechanics during ADL with PID-Controlled Dynamic Finite Element Analysis,” *Comput. Methods Biomech. Biomed. Engin.*, **17**(4).
- [35] van Eijden, T. M. G. J., de Boer, W., and Weijs, W. A., 1985, “The Orientation of the Distal Part of the Quadriceps Femoris Muscle as a Function of the Knee Flexion-Extension Angle,” *J. Biomech.*, **18**(10).

- [36] Blackburn, J. S., and Peel, T. E., 1977, “A New Method of Measuring Patellar Height,” *J. Bone Jt. Surg. - Ser. B*, **59**(2), pp. 241–245.
- [37] Reuben, J. D., McDonald, C. L., Woodard, P. L., and Hennington, L. J., 1991, “Effect of Patella Thickness on Patella Strain Following Total Knee Arthroplasty,” *J. Arthroplasty*, **6**(3), pp. 251–258.
- [38] Aguirre-Pastor, A., Ortolá, D. J., Lizaur-Utrilla, A., Rosa, M. A., and Lopez-Prats, F. A., 2020, “Is Pseudo-Patella Baja Really a Serious Complication of Total Knee Arthroplasty?,” *J. Arthroplasty*, **35**(2), pp. 557–562.
- [39] Behrend, H., Graulich, T., Gerlach, R., Spross, C., and Ladurner, A., 2019, “Blackburne–Peel Ratio Predicts Patients’ Outcomes after Total Knee Arthroplasty,” *Knee Surgery, Sport. Traumatol. Arthrosc.*, **27**(5), pp. 1562–1569.
- [40] Bugelli, G., Ascione, F., Cazzella, N., Franceschetti, E., Franceschi, F., Dell’Osso, G., Svantesson, E., Samuelsson, K., and Giannotti, S., 2018, “Pseudo-Patella Baja: A Minor yet Frequent Complication of Total Knee Arthroplasty,” *Knee Surgery, Sport. Traumatol. Arthrosc.*, **26**(6), pp. 1831–1837.
- [41] Gaillard, R., Bankhead, C., Budhiparama, N., Batailler, C., Servien, E., and Lustig, S., 2019, “Influence of Patella Height on Total Knee Arthroplasty: Outcomes and Survival,” *J. Arthroplasty*, **34**(3), pp. 469–477.
- [42] Chonko, D. J., Lombardi, A. V. J., and Berend, K. R., 2004, “Patella Baja and Total Knee Arthroplasty (TKA): Etiology, Diagnosis, and Management,” *Surg. Technol. Int.*, **12**, pp. 231–238.
- [43] Yang, J. S., Fulkerson, J. P., Obopilwe, E., Voss, A., Divenere, J., Mazzocca, A. D., and Edgar, C. M., 2017, “Patellofemoral Contact Pressures After Patellar Distalization: A Biomechanical Study,” *Arthrosc. - J. Arthrosc. Relat. Surg.*, **33**(11), pp. 2038–2044.
- [44] Luyckx, T., Didden, K., Vandenneucker, H., Labey, L., Innocenti, B., and Bellemans, J., 2009, “Is There a Biomechanical Explanation for Anterior Knee Pain in Patients with Patella Alta? Influence of Patellar Height on Patellofemoral Contact Force, Contact Area and Contact Pressure,” *J. Bone Jt. Surg. - Ser. B*, **91**(3), pp. 344–350.
- [45] Tischer, T., Geier, A., Lutter, C., Enz, A., Bader, R., and Kebbach, M., 2022, “Patella Height Influences Patellofemoral Contact and Kinematics Following Cruciate-Retaining Total Knee Replacement,” *J. Orthop. Res.*, (September 2021).
- [46] Ward, S. R., Terk, M. R., and Powers, C. M., 2005, “Influence of Patella Alta on Knee Extensor Mechanics,” *J. Biomech.*, **38**(12), pp. 2415–2422.
- [47] Fitzpatrick, C. K., Baldwin, M. A., Rullkoetter, P. J., and Laz, P. J., 2011, “Combined Probabilistic and Principal Component Analysis Approach for Multivariate Sensitivity Evaluation and Application to Implanted Patellofemoral Mechanics,” *J. Biomech.*, **44**(1), pp. 13–21.
- [48] Baldwin, M. A., Clary, C. W., Fitzpatrick, C. K., Deacy, J. S., Maletsky, L. P., and Rullkoetter, P. J., 2012, “Dynamic Finite Element Knee Simulation for Evaluation of Knee Replacement Mechanics,” *J. Biomech.*, **45**(3), pp. 474–483.
- [49] List, R., Schütz, P., Angst, M., Ellenberger, L., Dätwyler, K., Ferguson, S. J., von Eisenhart-Rothe, R., and Schwaller, C., 2020, “Videofluoroscopic Evaluation of the Influence of a Gradually Reducing Femoral Radius on Joint Kinematics During Daily Activities in Total Knee Arthroplasty,” *J. Arthroplasty*, **35**(10), pp. 3010–3030.
- [50] Dreyer, M. J., Trepczynski, A., Hosseini Nasab, S. H., Kutzner, I., Schütz, P., Weisse, B., Dymke, J., Postolka, B., Moewis, P., Bergmann, G., Duda, G. N., Taylor, W. R., Damm, P., and Smith, C. R., 2022, “European Society of Biomechanics S.M. Perren Award 2022: Standardized Tibio-Femoral Implant Loads and Kinematics,” *J. Biomech.*, **141**(June).
- [51] Willing, R., and Walker, P. S., 2018, “Measuring the Sensitivity of Total Knee Replacement Kinematics and Laxity to Soft Tissue Imbalances,” *J. Biomech.*, **77**, pp. 62–68.

- [52] ASTM Standard F3141-17a, 2018, “Standard Guide for Total Knee Replacement Loading Profiles.”
- [53] ISO 14243-1:2009, 2009, “Implants for Surgery - Wear of Total Knee-Joint Prostheses.”
- [54] Bourne, R. B., Chesworth, B. M., Davis, A. M., Mahomed, N. N., and Charron, K. D. J., 2010, “Patient Satisfaction after Total Knee Arthroplasty: Who Is Satisfied and Who Is Not?,” *Clin. Orthop. Relat. Res.*, **468**(1), pp. 57–63.
- [55] Parvizi, J., Nunley, R. M., Berend, K. R., Lombardi, A. V., Ruh, E. L., Clohisy, J. C., Hamilton, W. G., Della Valle, C. J., and Barrack, R. L., 2014, “High Level of Residual Symptoms in Young Patients after Total Knee Arthroplasty Knee,” *Clin. Orthop. Relat. Res.*, **472**(1), pp. 133–137.
- [56] Roussot, M. A., Vles, G. F., and Oussedik, S., 2020, “Clinical Outcomes of Kinematic Alignment versus Mechanical Alignment in Total Knee Arthroplasty: A Systematic Review,” *EFORT Open Rev.*, **5**(8), pp. 486–497.

Figure Captions List

- Fig. 1 Model of modified VIVO joint simulator retrofitted with custom fixturing and quadriceps actuation assembly (*left*). Axes labeled in blue highlight adjustment capabilities of the femoral fixture relative to the femoral coordinate system; joint simulator setup with fixtured TKA in synthetic bones (*middle*); finite element model of experimental configuration (*right*). Axes labeled in red are controlled by the joint simulator relative to the tibial coordinate system.
- Fig. 2 Assembly of the quadriceps clamp attached in-line with a linear actuator via a tensile load cell (*left*); Assembly of the instrumented patella fixture with 3-DoF piezoelectric load cell (*middle*); Diagram of the patella in the *alta* and *baja* configurations (*right*).
- Fig. 3 Finite Element model of the experimental configuration and the five alignment parameters that were perturbed in the sensitivity analysis
- Fig. 4 Mean patellofemoral reaction forces with 1000 N applied quadriceps force observed experimentally and predicted by the FE model at different knee flexion angles. Error bars indicate 1 standard deviation from the mean peak force during 3 experimental cycles.
- Fig. 5 Experiment and model tibiofemoral kinematics during a simple deep knee bending activity. Shaded regions indicate one standard deviation from the mean.
- Fig. 6 Femoral low-point A-P translation during the simple Deep Knee Bending activity. Experimental (solid) and computational (dashed) results are shown with *alta*, *neutral*, and *baja* tendon lengths. Shaded regions highlight one standard deviation from the mean.
- Fig. 7 Experimental (solid) and model (dashed) patellofemoral kinematics during a simple deep knee bending activity where all degrees of freedom except for flexion are in load control. Shaded regions highlight one standard deviation from the mean.

- Fig. 8 Comparison of patella implant positions between experimental (white) and model (green) configurations at 0°, 30°, 60°, and 80° of tibiofemoral flexion with *alta*, *neutral*, and *baja* patella positions
- Fig. 9 Experimental (solid) and Model (dashed) patellofemoral loads during the simple Deep Knee Bending activity for the *alta*, *neutral*, and *baja* tendon lengths. Shaded regions highlight one standard deviation from the mean.
- Fig. 10 Correlations between the FE model alignment perturbations and resulting knee mechanics at various flexion angles during a deep knee bend. Red regions indicate positive correlations while blue regions indicate negative correlations. Correlations less than 0.6 are shown in white. The slope of the linear fit is inset for variables with correlations greater than 0.6.
- Fig. 11 Model-predicted tibiofemoral loads during the simple Deep Knee Bending activity for the *alta*, *neutral*, and *baja* tendon lengths

Table Caption List

- Table 1 Root Mean Squared Error (RMSE), normalized Root Mean Squared Error (nRMSE), Mean Error (ME) and Standard Deviation (STD) of the differences between peak experimental and model P-F loads during sinusoidal loading of the quadriceps at 15°, 30°, 45°, and 60° knee flexion.
- Table 2 Root Mean Squared Error (RMSE), normalized Root Mean Squared Error (nRMSE), Mean Error (ME), and Standard Deviation (STD) of the error between experiment and model T-F and P-F kinematics during the simple Deep Knee Bending activity with *alta*, *neutral*, and *baja* tendon lengths.
- Table 3 Root Mean Squared Error (RMSE), normalized Root Mean Squared Error (nRMSE), Mean Error (ME), and Standard Deviation (STD) between experimental and model lowest point femoral condylar translations during the simple Deep Knee Bending activity with *alta*, *neutral*, and *baja* tendon lengths.
- Table 4 Root Mean Squared Error (RMSE), normalized Root Mean Square Error (nRMSE), Mean Error (ME), and Standard Deviation (STD) between experimental and model patellofemoral (P-F) loads during the simple Deep Knee Bend activity at *alta*, *neutral*, and *baja* tendon lengths.

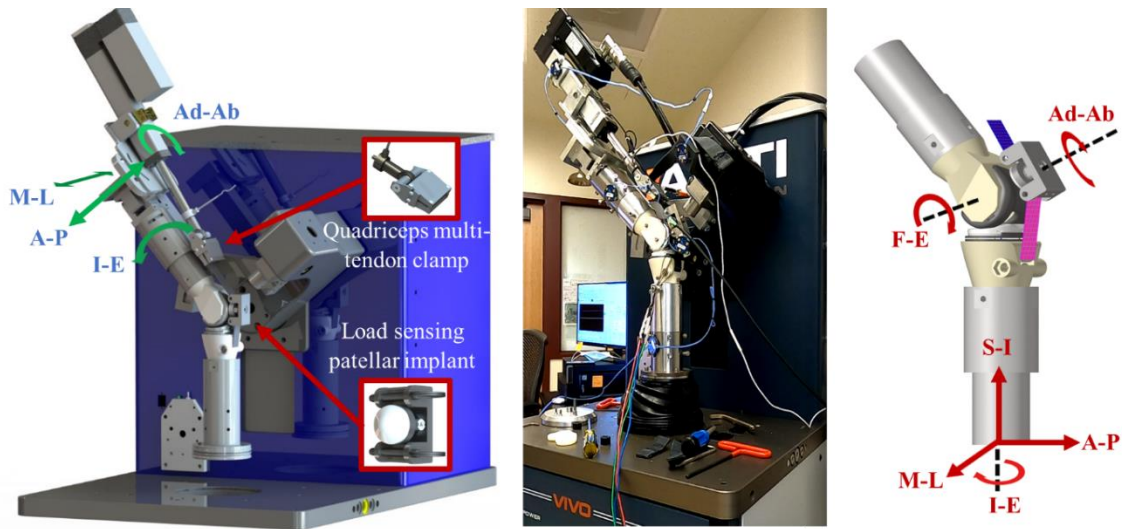


Figure 1: Model of modified VIVO joint simulator retrofitted with custom fixturing and quadriceps actuation assembly (*left*). Axes labeled in blue highlight adjustment capabilities of the femoral fixture relative to the femoral coordinate system; joint simulator setup with fixtured TKA in synthetic bones (*middle*); finite element model of experimental configuration (*right*). Axes labeled in red are controlled by the joint simulator relative to the tibial coordinate system.

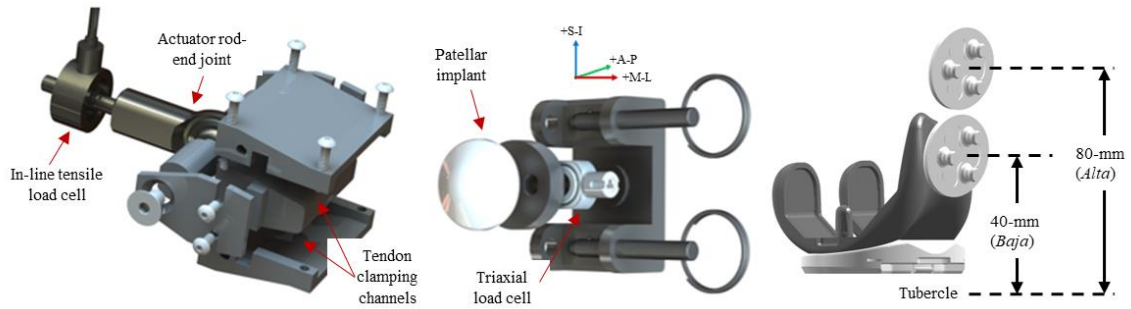


Figure 2: Assembly of the quadriceps clamp attached in-line with a linear actuator via a tensile load cell (*left*); Assembly of the instrumented patella fixture with 3-DoF piezoelectric load cell (*middle*); Diagram of the patella in the *alta* and *baja* configurations (*right*).

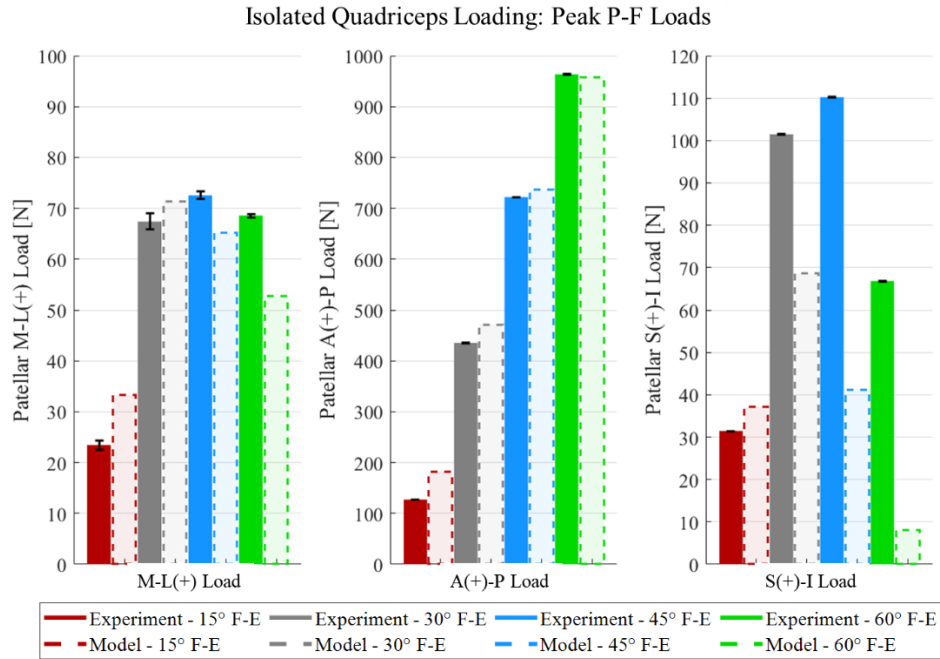


Figure 4: Mean patellofemoral reaction forces with 1000 N applied quadriceps force observed experimentally and predicted by the FE model at different knee flexion angles. Error bars indicate 1 standard deviation from the mean peak force during 3 experimental cycles.

Table 1: Root Mean Squared Error (RMSE), normalized Root Mean Squared Error (nRMSE), Mean Error (ME) and Standard Deviation (STD) of the differences between peak experimental and model P-F loads during sinusoidal loading of the quadriceps at 15°, 30°, 45°, and 60° knee flexion.

Patellofemoral Loads (N)

Knee Flexion	M-L				A-P				S-I			
	RMSE	nRMSE	ME	STD	RMSE	nRMSE	ME	STD	RMSE	nRMSE	ME	STD
15°	5.6	0.2	3.8	4.1	34.9	0.3	-24.7	24.7	5.2	0.2	-3.6	3.8
30°	5.2	0.1	-2.5	4.6	36.6	0.1	-7.3	35.9	20.5	0.2	17.1	11.3
45°	9.8	0.1	-9.0	3.9	49.9	0.1	11.0	48.7	42.6	0.4	35.7	23.4
60°	15.8	0.2	-15	5.1	65.7	0.1	26.9	60.0	40.6	0.6	33.5	22.9

Deep Knee Bending: T-F Kinematics

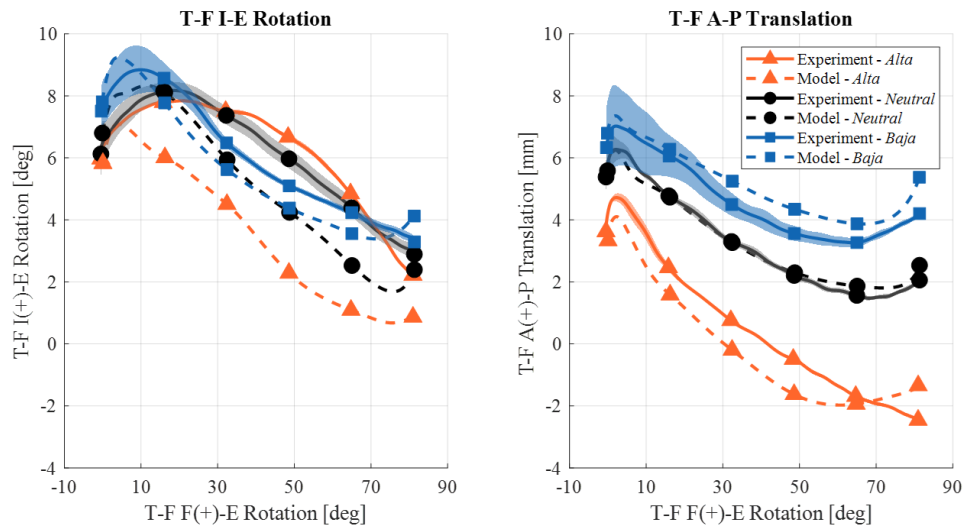


Figure 5: Experiment and model tibiofemoral kinematics during a simple deep knee bending activity. Shaded regions indicate one standard deviation from the mean.

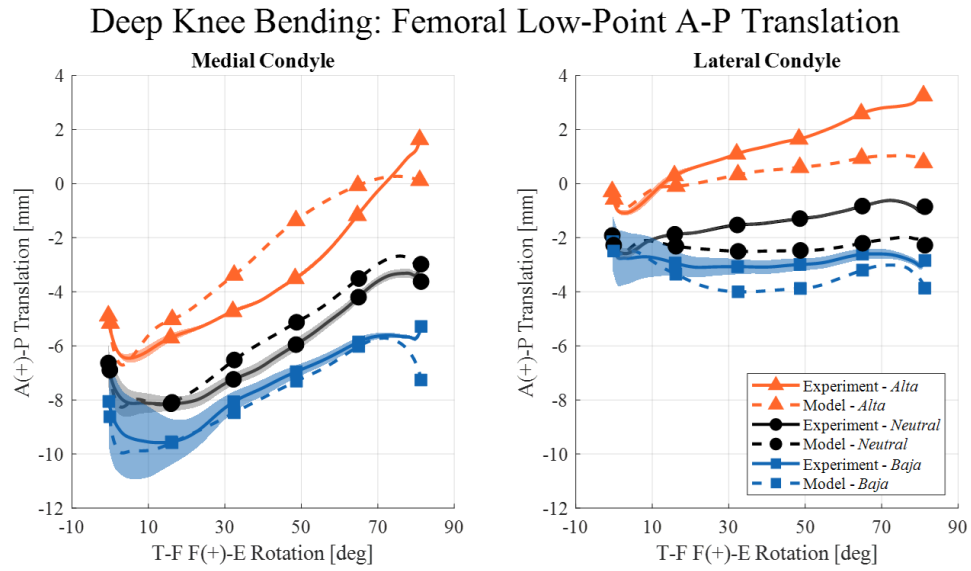


Figure 6: Femoral low-point A-P translation during the simple Deep Knee Bending activity. Experimental (solid) and computational (dashed) results are shown with *alta*, *neutral*, and *baja* tendon lengths. Shaded regions highlight one standard deviation from the mean.

Table 2: Root Mean Squared Error (RMSE), normalized Root Mean Squared Error (nRMSE), Mean Error (ME), and Standard Deviation (STD) of the error between experiment and model T-F and P-F kinematics during the simple Deep Knee Bending activity with *alta*, *neutral*, and *baja* tendon lengths.

		Rotations (deg)											
		F-E				V-V				I-E			
		RMSE	nRMSE	ME	STD	RMSE	nRMSE	ME	STD	RMSE	nRMSE	ME	STD
T-F	<i>alta</i>	1.1	0.0	-0.4	1.0	0.4	0.2	0.1	0.4	2.2	0.4	1.7	1.4
	<i>neutral</i>	1.1	0.0	-0.4	1.0	0.4	0.3	0.4	0.1	1.3	0.2	0.2	1.3
	<i>baja</i>	1.1	0.0	-0.4	1.0	0.4	0.3	0.4	0.2	1.3	0.2	-0.4	1.2
P-F	<i>alta</i>	2.3	0.1	-1.7	1.5	1.5	0.8	1.5	0.5	3.3	0.6	-2.8	1.7
	<i>neutral</i>	0.9	0.0	-0.6	0.7	0.8	0.3	-0.6	0.6	1.7	0.2	-0.9	1.4
	<i>baja</i>	2.0	0.0	-1.1	1.6	1.2	0.6	-0.8	0.8	3.3	0.6	-2.9	1.5
		Translations (mm)											
		M-L				A-P				S-I			
		RMSE	nRMSE	ME	STD	RMSE	nRMSE	ME	STD	RMSE	nRMSE	ME	STD
T-F	<i>alta</i>	1.7	0.9	1.6	0.8	0.7	0.1	0.1	0.7	0.5	0.5	0.2	0.2
	<i>neutral</i>	1.6	0.9	1.3	0.9	0.5	0.1	-0.2	0.4	0.3	0.2	0.3	0.3
	<i>baja</i>	1.6	1.0	1.4	0.8	0.8	0.2	-0.6	0.5	0.2	0.2	0.3	0.2
P-F	<i>alta</i>	1.3	0.5	1.1	0.7	0.8	0.1	0.2	0.8	1.2	0.0	0.2	1.1
	<i>neutral</i>	1.3	0.5	0.3	1.3	0.8	0.1	-0.1	0.7	0.7	0.0	0.6	0.3
	<i>baja</i>	1.4	0.3	1.2	0.7	0.7	0.0	0.0	0.7	1.3	0.1	0.7	1.0

Table 3: Root Mean Squared Error (RMSE), normalized Root Mean Squared Error (nRMSE), Mean Error (ME), and Standard Deviation (STD) between experimental and model lowest point femoral condylar translations during the simple Deep Knee Bending activity with *alta*, *neutral*, and *baja* tendon lengths.

Low Point Translation (mm)												
Medial Condyle												
	M-L				A-P				S-I			
	RMSE	nRMSE	ME	STD	RMSE	nRMSE	ME	STD	RMSE	nRMSE	ME	STD
<i>alta</i>	1.9	0.7	-1.7	0.9	1.1	0.1	0.1	1.1	0.6	0.4	-0.4	0.4
<i>neutral</i>	1.6	0.6	-1.3	1.0	0.8	0.2	0.1	0.8	0.5	0.8	0.4	0.2
<i>baja</i>	1.6	0.6	-1.2	1.0	1.2	0.2	0.8	0.9	0.6	0.9	0.5	0.2
Lateral Condyle												
	M-L				A-P				S-I			
	RMSE	nRMSE	ME	STD	RMSE	nRMSE	ME	STD	RMSE	nRMSE	ME	STD
<i>alta</i>	1.9	0.7	-1.7	0.9	1.3	0.3	1.1	0.7	0.4	0.9	-0.4	0.1
<i>neutral</i>	0.3	0.6	-1.1	0.8	0.8	0.4	0.7	0.4	0.3	0.4	-0.1	0.3
<i>baja</i>	0.3	0.5	-1.0	0.9	0.5	0.4	0.3	0.5	0.3	0.4	0.0	0.3

Deep Knee Bending: P-F Kinematics

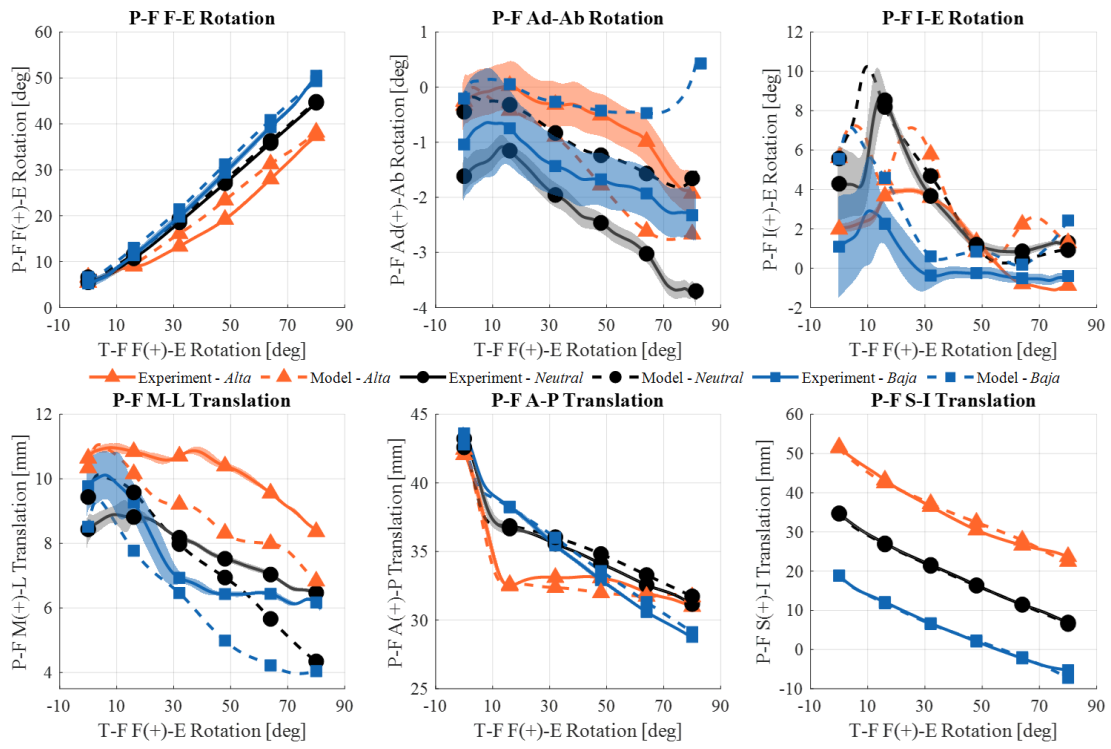


Figure 7: Experimental (solid) and model (dashed) patellofemoral kinematics during a simple deep knee bending activity where all degrees of freedom except for flexion are in load control. Shaded regions highlight one standard deviation from the mean.

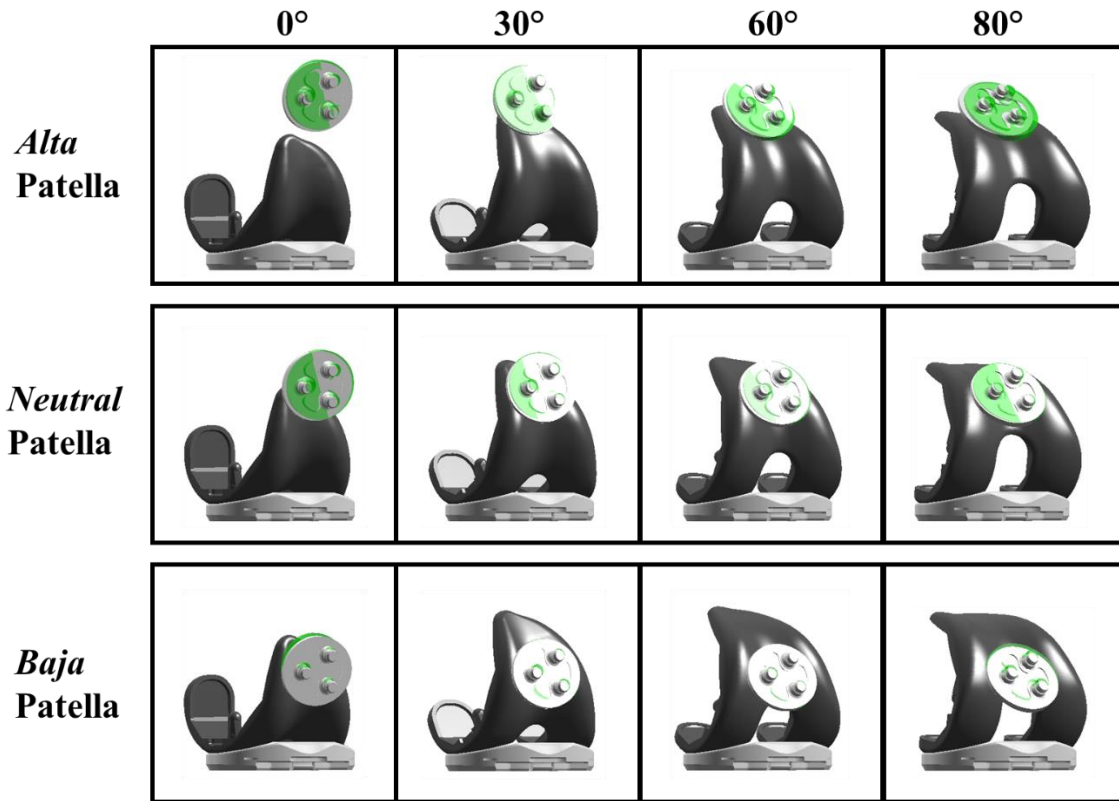


Figure 8: Comparison of patella implant positions between experimental (white) and model (green) configurations at 0°, 30°, 60°, and 80° of tibiofemoral flexion with *alta*, *neutral*, and *baja* patella positions

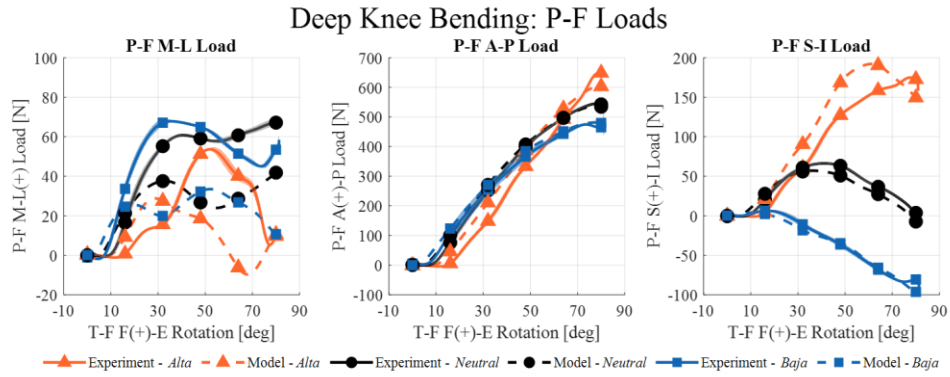


Figure 9: Experimental (solid) and Model (dashed) patellofemoral loads during the simple Deep Knee Bending activity for the *alta*, *neutral*, and *baja* tendon lengths. Shaded regions highlight one standard deviation from the mean.

Table 4: Root Mean Squared Error (RMSE), normalized Root Mean Square Error (nRMSE), Mean Error (ME), and Standard Deviation (STD) between experimental and model patellofemoral (P-F) loads during the simple Deep Knee Bend activity at *alta*, *neutral*, and *baja* tendon lengths.

Patellofemoral Loads (N)

	M-L				A-P				S-I			
	RMSE	nRMSE	ME	STD	RMSE	nRMSE	ME	STD	RMSE	nRMSE	ME	STD
<i>alta</i>	16.8	0.3	-4.3	16.3	53.6	0.1	-27.7	45.9	25.1	0.1	-10.2	23.0
<i>neutral</i>	17.1	0.3	-8.5	14.9	14.7	0.0	-5.8	13.5	7.4	0.1	3.4	6.6
<i>baja</i>	25.4	0.4	-16.4	19.4	14.4	0.0	-9.7	10.7	14.3	0.1	5.4	13.2

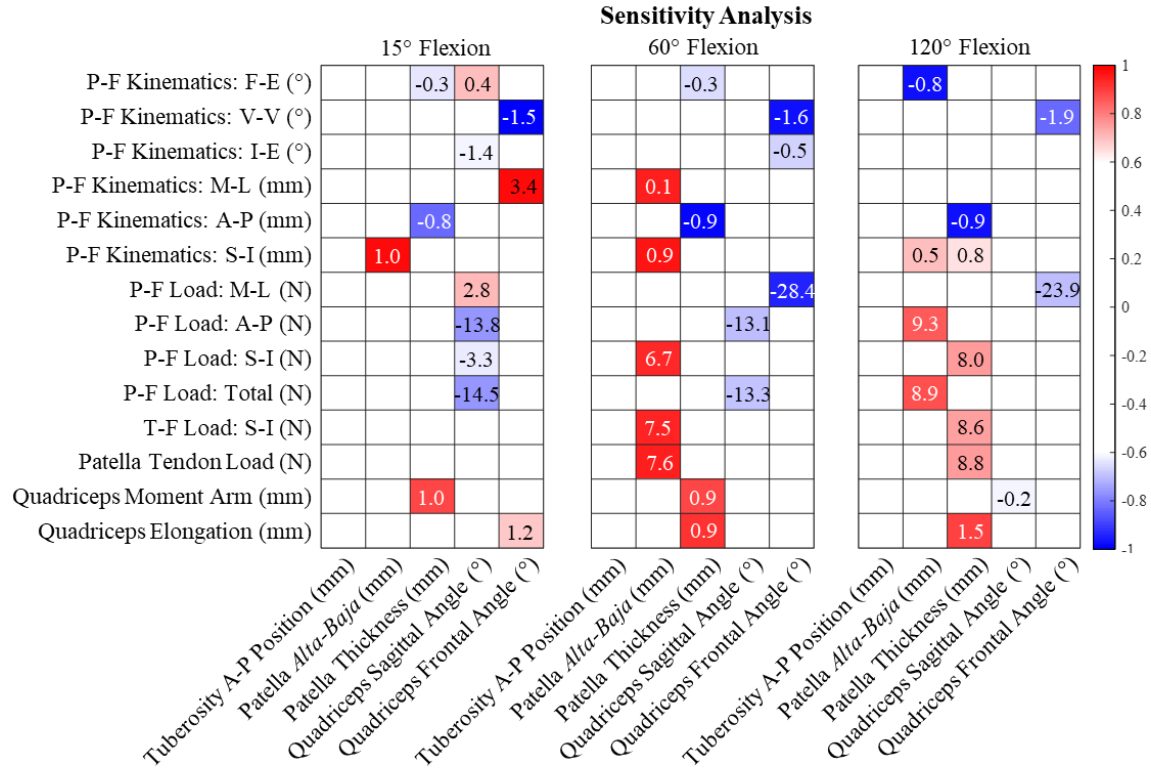


Figure 10: Correlations between the FE model alignment perturbations and resulting knee mechanics at various flexion angles during a deep knee bend. Red regions indicate positive correlations while blue regions indicate negative correlations. Correlations less than 0.6 are shown in white. The slope of the linear fit is inset for variables with correlations greater than 0.6.

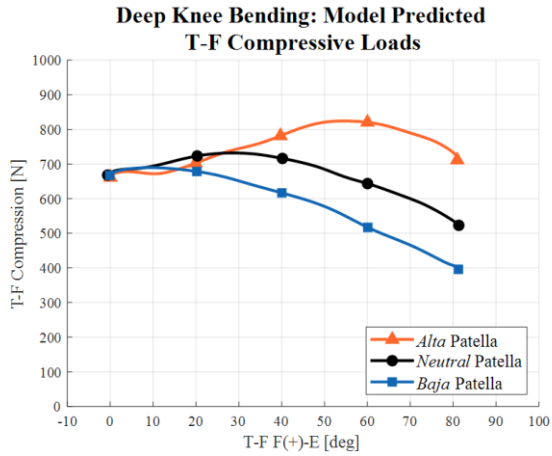


Figure 11: Model-predicted tibiofemoral loads during the simple Deep Knee Bending activity for the *alta*, *neutral*, and *baja* tendon lengths